The Astrophysical Journal, 720:757–770, 2010 September 1 doi:10.1088/0004-637X/720/1/757

DICHOTOMY OF SOLAR CORONAL JETS: STANDARD JETS AND BLOWOUT JETS

Ronald L. Moore[1], Jonathan W. Cirtain[1], Alphonse C. Sterling[1], and David A. Falconer[1,2,3]
[1] Space Science Office, VP62, Marshall Space Flight Center, Huntsville, AL 35812, USA; ron.moore@nasa.gov
[2] Physics Department, University of Alabama in Huntsville, Huntsville, AL 35899, USA
[3] Center for Space Plasma and Aeronomic Research, University of Alabama in Huntsville, Huntsville, AL 35899, USA
Received 2010 May 3; accepted 2010 June 23; published 2010 August 13

ABSTRACT

By examining many X-ray jets in *Hinode*/X-Ray Telescope coronal X-ray movies of the polar coronal holes, we found that there is a dichotomy of polar X-ray jets. About two thirds fit the standard reconnection picture for coronal jets, and about one third are another type. We present observations indicating that the non-standard jets are counterparts of erupting-loop Hα macrospicules, jets in which the jet-base magnetic arch undergoes a miniature version of the blowout eruptions that produce major coronal mass ejections. From the coronal X-ray movies we present in detail two typical standard X-ray jets and two typical blowout X-ray jets that were also caught in He II 304 Å snapshots from *STEREO*/EUVI. The distinguishing features of blowout X-ray jets are (1) X-ray brightening inside the base arch in addition to the outside bright point that standard jets have, (2) blowout eruption of the base arch's core field, often carrying a filament of cool ($T \sim 10^4 - 10^5$ K) plasma, and (3) an extra jet-spire strand rooted close to the bright point. We present cartoons showing how reconnection during blowout eruption of the base arch could produce the observed features of blowout X-ray jets. We infer that (1) the standard-jet/blowout-jet dichotomy of coronal jets results from the dichotomy of base arches that do not have and base arches that do have enough shear and twist to erupt open, and (2) there is a large class of spicules that are standard jets and a comparably large class of spicules that are blowout jets.

Key words: Sun: activity – Sun: corona – Sun: coronal mass ejections (CMEs) – Sun: magnetic topology – Sun: surface magnetism – Sun: transition region

1. INTRODUCTION

Solar X-ray jets, EUV jets, Hα surges, EUV macrospicules, and Hα macrospicules are similar columnar eruptions that are magnetically rooted in the photosphere and shoot up into the corona. In this paper, we refer to all of these eruptions as coronal jets. (Although Hα surges and Hα macrospicules are commonly and appropriately called chromospheric jets, here we include them under our umbrella term coronal jets for simplicity of presentation, and because they appear to be similar to other coronal jets in their magnetic setting and generation.) The main difference between the above listed subclasses of coronal jets is in the nominal temperature of the ejected plasma ($\sim 4 \times 10^6$ K for X-ray jets, $\sim 10^5$ K for EUV jets and EUV macrospicules, and $\sim 10^4$ K for Hα surges and Hα macrospicules), although the temperature range of the ejected plasma varies so greatly from event to event within each subclass that any given event of one subclass might or might not be also observable as a member of any other subclass (e.g., see Shibata 2001). Across these subclasses, the eruptions are largely similar in form and motion, and this similarity suggests that they might all be generated in the same way. Each has basically the same magnetic field setup in that each shoots up along a large-scale unipolar guide field that reaches high into the corona, and in that each is rooted around an inclusion of opposite-polarity magnetic flux of the diameter of the base of the jet. Typically, most of the opposite-polarity flux is in one foot of a small magnetic arch that has emerged or is still emerging from below the photosphere. This, the explosive character of these eruptions, and the inverted-Y or Eiffel-tower shape of many jets, surges, and macrospicules point to sudden reconnection at the interface between the unipolar ambient field and the opposite-polarity leg of the arch as the basic mechanism that produces these eruptions (Shibata et al. 1992; Shibata 2001). In this scenario, the interior of the arch remains quasi-static during the burst of reconnection of some of the arch's outer field with the ambient field. In this paper, we refer to this reconnection scenario as the standard model for solar coronal jets. Jets and macrospicules that fit this model we call standard jets.

Macrospicules are so named because they are reminiscent of the much smaller chromospheric spicules. Spicules are rooted in the magnetic network in quiet regions and coronal holes, have widths ranging below $\sim 10^3$ km, reach to heights of 5–10 $\times$ 10^3 km above the photosphere, and make up most of the $T \sim 10^4$ K chromosphere at heights above 2–3 $\times$ 10^3 km (Beckers 1968, 1972; Sterling 2000). The Solar Optical Telescope (SOT) on *Hinode* has taken Ca II H movies of the spicule forest at the limb with unprecedented continuous 0.2 arcsec resolution. These movies show that much of the forest is spicules that are narrower, briefer, and three to four times faster than the spicules previously detected in less well resolved chromospheric movies (e.g., De Pontieu et al. 2007; Sterling et al. 2010). These fast spicules erupt upward at speeds of ~ 100 km s^{-1}. In the spicule movies from SOT, it is not obvious how the fast spicules are generated, but the ubiquity of the fast spicules in these movies and recent follow-up observational and MHD modeling work encourage the view long advocated by many researchers that fine-scale explosive magnetic activity involving reconnection low in the network powers coronal heating and the solar wind in quiet regions and coronal holes (e.g., Rabin & Moore 1980; Porter & Moore 1988; Parker 1991; Moore et al. 1991, 1999; Axford & McKenzie 1992; Schrijver et al. 1998; Falconer et al. 1998, 2003; Fisk et al. 1999; McIntosh et al. 2007; Heggland et al. 2009; Rouppe van der Voort et al. 2009; Roberts 2010). To the extent that coronal jets are larger versions of the fast spicules, how coronal jets are generated bears on how fast spicules are generated and on whether this is the magnetic activity that sustains the global corona and solar wind.

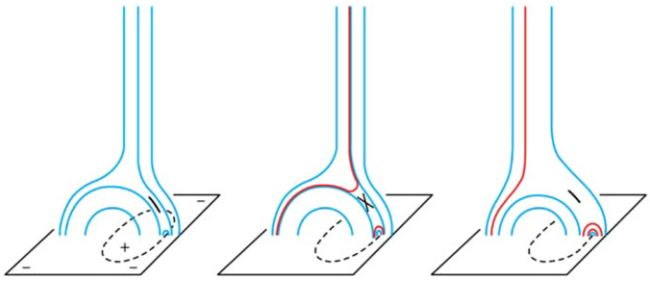

Figure 1. Sequence of cartoons portraying the topology and reconnection of the magnetic field in the standard model for solar coronal jets. Only a few representative field lines (blue or red) are drawn. Left: the field configuration before the burst of reconnection that produces the jet. The dashed oval is the polarity inversion line around the positive flux of the emerging magnetic arch. The nearly unstable portion of the current sheet between the emerging closed field and the ambient open field is represented by the curved black line segment. Middle: the growing jet early in the burst of reconnection that occurs in the disrupted current sheet and that is symbolized here by the slanted X. Red field lines are reconnected ones that have reconnection-heated hot plasma on them. Blue field lines either have yet to or will not undergo reconnection. Right: the decaying jet immediately after the burst of reconnection has ended.

Yamauchi et al. (2004) studied the structure of Hα macrospicules at the limb in polar coronal holes. Within the polar coronal holes present during the 1996–1997 minimum epoch of the solar cycle, they searched 6 days of Big Bear Solar Observatory full-disk Hα movies for macrospicules that were at the limb and were observed from beginning to end. They found 35 such macrospicules and examined the structure and development of each. Nearly half (17) had the inverted-Y form of standard jets, and so were plausibly produced by reconnection in the manner of the standard model. But nearly as many (15) were not of this form, but had the form of a small erupting loop. These eruptions appear similar to the eruption of the core-field filament in the much larger eruptions that produce major coronal mass ejections (CMEs). For example, the erupting-loop macrospicule shown in Figure 3 of Yamauchi et al. (2004) erupted in the manner of the filament in the CME eruption onset shown in Plate 1 of Moore & Sterling (2006). Only about 10% of the macrospicules (3) had structure that could not be discerned to be of either the standard-jet type or the erupting-loop type. Thus, Yamauchi et al. found that there is a dichotomy of Hα macrospicules, the standard-jet type and the erupting-loop type, which evidently differ in how they are produced.

If, as their general similarity in form and motion suggests, Hα macrospicules and X-ray jets are basically the same kinds of magnetic eruptions, differing in temperature but produced by the same magnetic arrangement, then the observation that at least a large minority of Hα macrospicules are not standard jets but erupting loops suggests that there should be many X-ray jets that are not standard jets but instead are counterparts of erupting-loop Hα macrospicules. We looked for such non-standard X-ray jets by examining the structure and development of many X-ray jets that occurred in the polar coronal holes in 2008, during the middle of the most recent (2007–2009) minimum epoch of the solar cycle. The observations that we studied are coronal X-ray movies from the X-Ray Telescope (XRT) on *Hinode*. These movies have 1 arcsec pixels and cadence of 1–2 minutes. We found that most X-ray jets have structure and development that fit the standard model, but that many X-ray jets are of another type. X-ray jets of this other type have certain features during their growth phase that are not expected from the standard model, but that plausibly would be produced by eruption of the base magnetic arch as in an erupting-loop Hα macrospicule.

In this paper, we present two typical standard X-ray jets and two typical X-ray jets of the other type. Each occurred on a separate day during a several-hour XRT movie of the north or south polar coronal hole. We selected these four events because each was also caught in EUV snapshots from the EUV Imager (EUVI) on each of the two spacecraft of the *STEREO* mission. For each of our four events, during the X-ray jet's growth phase and/or maximum phase, there is an EUVI He II 304 Å image from the *STEREO A* spacecraft (flying ahead of the Earth in Earth's orbit around the Sun) and an EUVI He II 304 Å image from *STEREO B* (lagging the Earth). These are full-disk images with 1.6 arcsec pixels. Because the cadence of the EUVI He II 304 Å images is typically no faster than 10 minutes and the growth phase of most X-ray jets lasts only a few minutes, growing X-ray jets observed by XRT are usually missed by the EUVI He II 304 Å snapshots. The four X-ray jets that we present are the best four that we have found for how well the middle of the development of each was caught in these snapshots. From (1) the signature features of the jets of the non-standard type observed in the coronal X-ray movies, and (2) further evidence from the He II 304 Å images that the base arch did not erupt in the two example standard X-ray jets, but did erupt as in a CME eruption in the two example X-ray jets of the non-standard type, we infer that such non-standard jets correspond to erupting-loop Hα macrospicules. Because in this type of coronal jet the base arch does not remain static and closed as in a standard jet but explodes open as in a CME eruption, we call these "blowout jets."

We also found that most X-ray jets are either standard jets or blowout jets, and that this dichotomy is more lopsided than the corresponding dichotomy of Hα macrospicules found by Yamauchi et al. (2004). To obtain an unbiased estimate of the relative population of standard X-ray jets, blowout X-ray jets, and X-ray jets that are not discernibly either of these two types, we examined the structure and development of each obvious jet observed in the four XRT movies in which we found our four example jets. In the total of 40 hr covered by these four movies, we found 55 jets. Of these, 34 appeared to be standard jets, 18 appeared to be blowout jets, and 3 could not be discerned to be of either type. Evidently, about two thirds of all X-ray jets in polar coronal holes are standard jets, and about a third are blowout jets.

2. STANDARD JETS

2.1. Standard Model

Figure 1 schematically depicts the standard reconnection scenario for coronal jets. This is basically the scenario that Shibata et al. (1992) deduced from the structure and development of typical jets observed in coronal X-ray snapshots and movies from the Soft X-ray Telescope (SXT) on *Yohkoh*.

In the drawing on the left in Figure 1, a small bipolar magnetic arcade or fat arch has emerged into surrounding unipolar high-reaching field such as the open field in a coronal hole. The magnetic arch is like the field of a simple bipolar active region, only smaller. In the depicted case, the polarity of the ambient field is negative; the direction of the field is downward. The intrusion of the arch field has forced a current sheet to form. The current sheet is between the arch and the ambient field, at the interface where the positive-polarity leg of the arch presses against oppositely directed ambient field. In this drawing, we have assumed that some time earlier reconnection at this interface produced the small magnetic loop over the

inversion line between the positive flux of the arch and the ambient negative flux.

In the version of the standard scenario depicted in Figure 1, there is no twist in the magnetic field and hence no electric current either inside the emerging arch or outside in the ambient field. So, all of the free magnetic energy in this setup is due to the formation of the current sheet. In the state depicted on the left in Figure 1, the current sheet is stable against reconnection, but close to being unstable. As the magnetic arch gradually continues to emerge, a portion of the current sheet is forced to become thin enough to be unstable to reconnection. This results in a burst of reconnection that releases some of the built-up free energy of the field around the current sheet. In the middle drawing in Figure 1, this burst of reconnection has started. The reconnection heats the plasma on the reconnected field lines to several million degrees, hot enough to emit strongly in the soft X-ray emission observable by *Yohkoh*/SXT and *Hinode*/XRT. The reconnected field lines that are released upward by the reconnection are open field lines that are rooted in the reconnected negative flux of the arch. The spire of the jet is the hot plasma escaping upward along the reconnected open field lines. The reconnected field lines that are released downward by the reconnection are new closed field lines that form a miniature X-ray flare arcade over the polarity inversion line at the outer edge of the positive flux of the emerging magnetic arch. In coronal X-ray images from XRT, this miniature flare arcade is typically seen as a "bright point" at the minority-polarity end of the arch (Savcheva et al. 2007, 2009). In this scenario, the reconnection process produces no appreciable plasma heating either on upstream field lines before they undergo reconnection or on nearby field lines that are beside the inflow to the patch of reconnection and do not undergo reconnection; only the reconnected field lines have had their plasma heated enough to be bright in X-ray emission.

As the burst of reconnection peaks, the X-ray jet spire attains its maximum brightness, height, and width, and the base-edge bright point attains its maximum brightness and area. During the maximum phase of the jet, the spire usually migrates laterally away from the bright point (Savcheva et al. 2007, 2009). The spire and the bright point fade as the reconnection slows and stops. Presumably, the reconnection stops when it has removed enough of the compressed field pressing on the current sheet for the current sheet to again be stable against reconnection. The drawing on the right in Figure 1 depicts the jet at the end of the burst of reconnection. Here, relative to the corresponding feature in the middle drawing, the bright point is larger, the spire is farther from the bright point, and reconnection at the current sheet has stopped.

Most aspects of standard jets portrayed in Figure 1 and described above have been demonstrated in two-dimensional simulations (Yokoyama & Shibata 1996) and in three-dimensional simulations (Moreno-Insertis et al. 2008) in which a magnetic arch in which the field has no significant twist emerges through the photosphere into ambient unipolar open field. In agreement with Figure 1, these simulations show the current sheet building up between the ambient field and the opposite-polarity leg of the arch, the burst of reconnection at the current sheet, and the resulting spire and bright point of the X-ray jet. In these simulations, the patch of current sheet in which reconnection occurs is small relative to the whole emerging arch, roughly as in Figure 1. The only characteristic shown in Figure 1 that is not borne out by both of these two simulation studies is the drift of the spire away from the bright point. In the two-dimensional simulation of Yokoyama & Shibata (1996) shown in their Figure 12, the spire does move laterally away from the bright point, but in the three-dimensional simulation of Moreno-Insertis et al. 2008, the spire drifts toward the bright point as the reconnection progresses.

For standard jets, we expect that the size of the emerging magnetic arch should be a major determinant of the temperature of the plasma in the spire of the jet. In standard X-ray jets, the arch usually spans ∼20,000 km or more (Shimojo et al. 1996), and so arches well above the ∼5000 km height of the chromosphere and transition region. For jet-base arches this big, simply because most of the interface with the ambient field is in the low corona, the jet-producing reconnection most likely takes place in the low corona. When the reconnection is in the low corona, the plasma on the field lines in the inflow to the reconnection already has a temperature of $\sim 10^6$ K and the reconnection makes it hotter. In such cases, the spire should be strongly visible in coronal X-ray images and hardly or not at all visible in EUV and Hα images, because the spire should have lots of plasma at X-ray temperature and little in the temperature range of the chromosphere and transition region (10^4–10^6 K). This preponderance of X-ray plasma in the jet spire when the reconnection is in the low corona is demonstrated in the simulations of standard jets by Yokoyama & Shibata (1996) and Moreno-Insertis et al. 2008. For some jet-base arches that are big enough to arch well into the low corona, details of the structure and evolution of the field might result in the reconnection taking place down in the transition region and/or the chromosphere instead of up in the low corona. When this happens, most of the plasma on the field lines flowing into reconnect will be at transition-region and chromospheric temperatures. This could result in much of the plasma expelled on the upward released reconnected field lines being at these sub-coronal temperatures. Because most standard jets have base arches spanning ∼20,000 km or more, we expect that it is unusual for standard X-ray jets to have their reconnection in the transition region and chromosphere. Therefore, we expect that most standard X-ray jets are much more visible in coronal X-ray images than in EUV or Hα images. Conversely consistent with this, the span of the jet-base magnetic arch in Hα macrospicules of the standard-jet type is nearly always less than 10,000 km (Yamauchi et al. 2004). For these arches, little or none of the interface with the ambient field is above the chromosphere. For standard jets that have base arches this small, we expect that most of the plasma ejected up into the spire is usually mostly of chromospheric or transition-region temperature, and hence that these jets are usually much less visible as X-ray jets than as Hα or EUV jets. This cool-spire consequence of the span of a jet-base arch being ∼10,000 km or less would explain why the X-ray component of the Hα surge observed by *Yohkoh*/SXT and shown in Shibata et al. (1992) was small and weak. This Hα surge was of the standard-jet type, had a base-arch span of about 10,000 km, and was much larger and longer lasting in Hα images than in the SXT coronal X-ray images.

2.2. Standard X-ray Jet of 2008 September 22

In this section, we present the first of our two example standard X-ray jets observed by *Hinode*/XRT. This jet is from a movie taken by XRT on 2008 September 22. The movie views much of the northern polar corona hole, has 1 minute cadence, and was taken with the Thin Al Poly filter. XRT images taken with this filter show solar plasma that is hotter than 10^6 K,

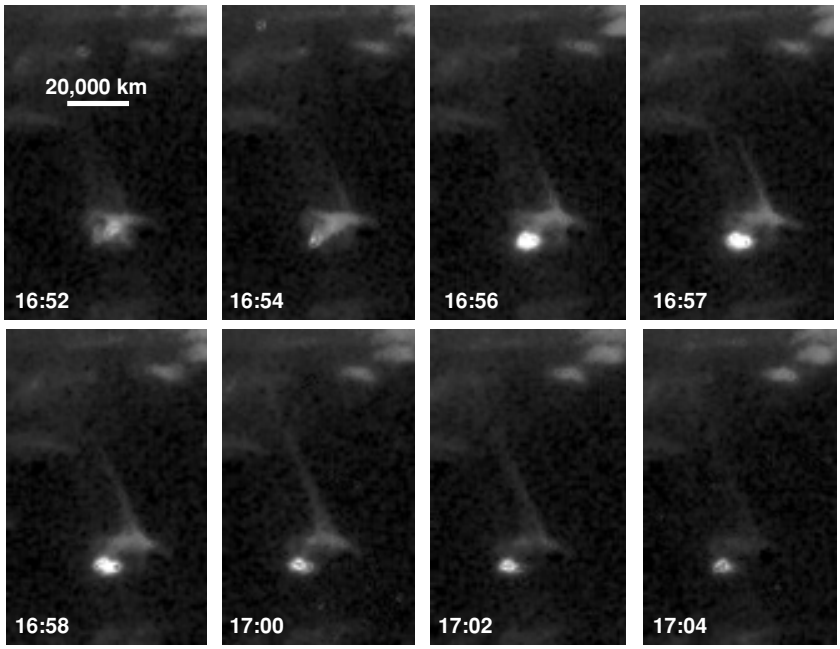

Figure 2. Progression of the standard jet of 2008 September 22 observed in coronal X-ray images from *Hinode*/XRT. In these images and in all other images in this paper, solar north is up and west is to the right. The jet is near central meridian in the northern polar coronal hole. The limb is just inside the north (top) edge of the field of view. The 20,000 km bar shows that this jet's base arch spans about 20,000 km. In the lower left of each frame is the universal time in hours and minutes.

and are insensitive to cooler plasma (Kano et al. 2004; DeLuca 2007). Figure 2 shows the jet in a small sub field of view of the movie. The time spanned by this sequence of selected frames is from before the onset of the jet through most of the decay phase.

The magnetic arch that produced this jet is seen in the first frame of Figure 2, at about 2 minutes before the jet starts. The arch is tilted from east–west: its western end is northwest of its eastern end. As can be seen from the length scale, the outer edge of the arch spans about 20,000 km. In the first frame, the arch is brightest in its interior. In addition to this bright arch, a decaying previous jet, extending upward from the arch, is faintly visible in the first frame. This faint jet is not clearly a standard jet. In the second frame, 2 minutes later, the faint previous jet has faded, the interior of the base arch dims, and the spire and bright point of our example standard jet turn on. The spire stems from the northwest leg of the base arch, and the bright point is at the other end of the arch. The interior of the arch continues to dim throughout the rest of the sequence. In the third frame, 2 minutes after the second frame, the bright point has grown larger and much brighter, and the spire has grown brighter and taller. In the fourth frame, 1 minute later, the bright point has changed only a little while the spire has continued to grow brighter and taller. A minute later, in the fifth frame, the bright point has started to decay while the spire has grown taller and thicker but not brighter. Two minutes later, in the sixth frame, the spire has grown still bigger. Finally, as the bright point continues to decay, the spire decays during the next 4 minutes (seventh and eighth frames). Throughout the event, the diameter of the bright point and the width of the spire are small compared to the span of the base arch. Perhaps because this jet's base arch is viewed end-on nearly as much as side-on, this jet's spire shows little or no lateral drift.

The structure and development of this jet fit the standard model well. The spire and the bright point were at opposite ends of the base arch; they turned on and grew in synchrony; they were much smaller in lateral span than the base arch; and there was no discernible heating of X-ray plasma in the interior of the arch as the jet grew. As is sketched in Figure 1, these features are those expected if the jet were made by a burst of reconnection at a small patch of the interface between the ambient open field of the coronal hole and the opposite-polarity leg of the base arch, and if the interior of the base arch remained quasi-static during the burst of reconnection.

Because the magnetic-arch base of this jet had a span of 20,000 km, if the jet was produced by reconnection as in the standard model, then it is reasonable that this reconnection occurred in the low corona, and hence that plasma in the reconnection outflow was many times hotter than 10^6 K, making the jet clearly visible in the XRT images in Figure 2. The downward product of the reconnection, the bright point, is a miniature flare arcade in which the downward reconnection-heated plasma is trapped. This X-ray plasma is in thermal contact with the transition region and chromosphere at the feet of this arcade. Therefore, as in larger flare loops, the feet of the bright point should first brighten in EUV emission from plasma at temperatures of $\sim 10^6$ K and less, and later the body of the bright point should become visible in this emission as its loops cool below 10^6 K. The upward outflow from the reconnection generates the jet's spire. This reconnection-heated plasma has thermal contact with the transition region and chromosphere at the feet of the reconnected open field lines. This should heat and "evaporate" the plasma there, making a "flare ribbon" in EUV emission from plasma at temperatures of $\sim 10^6$ K and less at the foot of the spire. Because, at least at first, the rest of the spire should be hotter than 10^6 K, it should be much more visible in soft X-ray emission than in EUV emission from cooler plasma.

Figure 3 shows that our present example standard jet displayed the above expected signatures. The XRT image in Figure 3 shows the jet and its surroundings in 5–50 Å soft X-ray emission from plasma at temperatures well above 10^6 K (Kano et al. 2004; DeLuca 2007). The EUVI 195 Å images in Figure 3 show the same heliographic area in Fe XII emission from $\sim 1.5 \times 10^6$ K plasma, and the EUVI 304 Å images show this area in He II emission from $\sim 8 \times 10^4$ K plasma (see Howard et al.

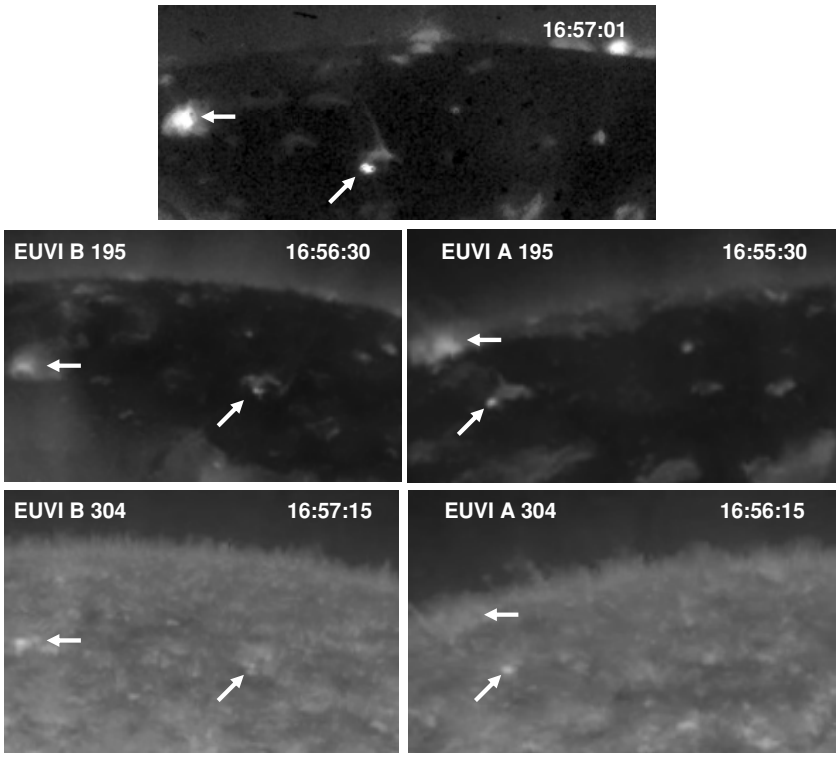

Figure 3. Co-temporal snapshots of the standard jet of 2008 September 22 showing that nearly all of the plasma in the jet's spire was hotter than $\sim 1.5 \times 10^6$ K. Top: XRT image of the jet and its surroundings in the northern polar coronal hole. This is a larger sub field of view taken from the same frame of the XRT movie as the fourth frame of Figure 2. It shows the jet when the bright point was near its peak in size and brightness. Middle left: EUVI B 195 Å image of about the same heliographic area viewed in the top image. Middle right: EUVI A 195 Å image of roughly the same heliographic area. Bottom left: EUVI B 304 Å image of nearly the same area viewed in the EUVI B 195 Å image above it. Bottom right: EUVI A 304 Å image of nearly the same area viewed in EUVI A 195 Å image above it. In each image, the slanted arrow points to the jet's bright point, the horizontal arrow points to the X-ray-bright ephemeral active region seen in the top image, and the universal time is in the upper right corner. The angle of separation from Earth was 39° for *STEREO A* and 35° for *STEREO B*.

2008 for EUVI's plasma–temperature response curves). All of these snapshots are within a 1.75 minute interval during the jet's growth phase as seen in Figure 2. The jet's base, especially the bright point, is visible in each of the four EUVI snapshots. Most of this brightening in the EUVI images appears to be either low in the bright point seen by XRT or at the foot of the spire. The spire is clearly visible in the XRT image, but is not visible in either of the He II 304 Å images, and shows at most only a faint rudiment in the Fe XII 195 Å images. These observations signify that this jet was produced by a burst of reconnection in the low corona at the outer edge of the base arch as in the standard model, and that, also in accord with the standard model, during the burst of reconnection the interior of the arch remained quasi-static and underwent no appreciable heating as the jet was produced.

2.3. Standard X-ray Jet of 2008 October 5

The development of our other example standard X-ray jet is shown in the sequence of XRT images in Figure 4. These frames show the jet in a small sub field of view from an XRT movie that views much of the northern polar coronal hole for several hours on 2008 October 5. The movie was taken with the Thin Al Poly filter and has 1 minute cadence. The movie covers the onset of this jet and its growth into its maximum phase, and then has a 26 minute gap during which the jet ends.

In the first frame of Figure 4, the jet gradually starts; the spire is short and quite faint. The spire stems from the top of the base arch and slants to the south with the field of the coronal hole. The base arch is viewed nearly side-on, and spans about 15,000 km. In the first frame, the whole base arch is bright, but its southwest leg is brighter than its northeast leg. In the second frame, 3 minutes later, each leg has brightened a little and so has the spire. Two minutes later (third frame), each leg has brightened a little more and the spire is a little larger. In another 2 minutes (fourth frame), while the southwest leg of the arch is hardly any brighter, the expected miniature-flare-arcade bright point for standard jets has become obvious at the northeast end of the base arch, and the spire is bigger and brighter. During the growth of the jet from the first frame to the fourth (7 minutes), the spire drifts laterally away from the bright-point end of the base arch, as can be seen by the migration of the spire relative to the small bright feature behind it on the limb. In the fifth frame (1 minute after the fourth frame), the southwest leg of the base arch has hardly changed in brightness, but the bright point is noticeably bigger and brighter, and the spire is longer and has reached its maximum brightness. Over the next 5 minutes (sixth and seventh frames), the southwest leg of the base arch dims while the bright point and the spire continue growing. In the seventh frame, the bright-point arcade has become nearly half as wide as the base arch. In the eighth and last frame (from the first frame of the movie after the gap), the spire is gone but a remnant of the bright point and some inner loops of the base arch are still bright enough to be seen, but are much dimmer than before the gap.

This jet fits the standard model about as well as our other example standard jet, except that here the interior of the base arch apparently was not entirely inert but had an episode of activity

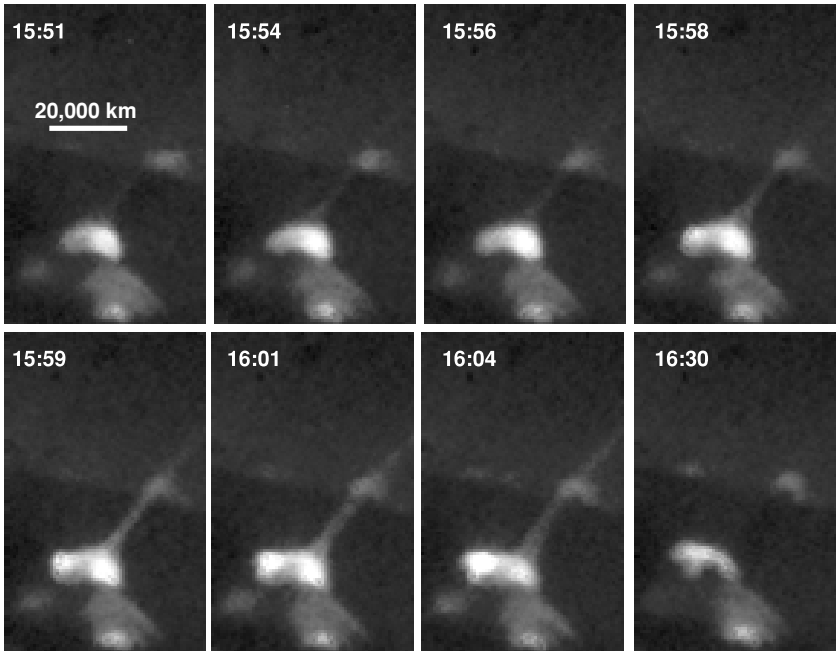

Figure 4. Progression of the standard jet of 2008 October 5 observed in coronal X-ray images from *Hinode*/XRT. The jet is near the northwest limb in the northern polar coronal hole. The jet's base arch is viewed side-on and spans about 15,000 km. Each frame has its universal time in the upper left.

in its southwest leg that heated plasma to X-ray temperatures as the jet started. This transient heating activity perhaps triggered the jet-producing burst of reconnection at the outer edge of the northeast leg of the base arch. Even if this internal activity of the base arch disturbed the interface current sheet enough to trigger the reconnection, it is unlikely that the internal activity was the main driver of the reconnection, because the bright point and the spire continued to grow as the base arch's internal heating decayed. More likely, most of the free energy released by the reconnection was already stored in the compressed field around the current sheet, by gradual buildup prior to the base arch's episode of internal activity. In any case, in Figure 4, the base arch remains largely intact during the production of the jet. It shows no sign of erupting open in the manner of the erupting arcade enveloping an erupting filament in a CME.

Because the base arch spanned 15,000 km and the bright point grew to have almost half that span, most of the reconnection probably occurred in the low corona, at a patch high on the northeast leg of the base arch. Thus, from Figure 4 alone, it seems likely that nearly all of the plasma in this jet's spire was at temperatures well above 10^6 K. This expectation is borne out by Figure 5. Figure 5 for this standard jet corresponds to Figure 3 for our other example standard jet, except in place of the EUVI 195 Å filtergrams in Figure 3, Figure 5 has EUVI 284 Å filtergrams. The EUVI 284 Å filtergrams show Fe XV emission from $\sim 2 \times 10^6$ K plasma (Howard et al. 2008). The five snapshots in Figure 5 are all within a 3.33 minute interval that begins in the maximum phase of the jet. The jet's bright point and base arch are visible in both of the EUVI 284 Å images, but the spire is too faint in Fe XV 284 Å emission to be seen in either. The bottom of the bright point and the bottom of the base arch are visible in the EUVI A 304 Å image. They are not visible in the EUVI B 304 Å image, probably because the jet is so near the limb from the perspective of EUVI B that the low layers bright in 304 Å emission are obscured by the foreground chromosphere and transition region. The jet's spire is not visible in either 304 Å snapshot. Thus, Figure 5 confirms that the plasma in this jet's spire was practically all hotter than $\sim 2 \times 10^6$ K, consistent with the inference from Figure 4 that the jet-producing reconnection occurred in the corona low above the transition region.

3. BLOWOUT JETS

As was stated at the end of Section 1, we have found that about two thirds of all X-ray jets observed by *Hinode*/XRT in the polar coronal holes have structure and development that fit the standard model. Nearly all of the rest, about a third, are of another type. Based on their observed characteristics, we think that "blowout jets" is a good name for jets of this type. In this section, we present two representative examples of these non-standard jets. Each of these shows the basic characteristics of this type of jet in XRT images. In addition, each was caught in EUV images taken by EUVI A and EUVI B. These EUVI snapshots show that, in addition to the X-ray-emitting plasma seen by XRT, a lot of much cooler plasma erupted up along the spire of the X-ray jet. The observed structure and timing of these cooler ejecta suggests that this plasma erupted from low in the jet's base arch, in an ejective eruption of the magnetic field in the core of the arch as in a filament eruption in a CME. We therefore propose that whether an X-ray jet is a standard jet or is of this non-standard type is determined by whether the base arch remains closed or erupts open, i.e., blows out, during the production of the jet. In Section 3.3, we present cartoons that show how the non-standard X-ray structure of a blowout jet could be produced by the ejective eruption of the base arch.

3.1. Blowout X-ray Jet of 2008 September 20

The sequence of coronal X-ray images in Figure 6 shows the development of our first example blowout jet. The sequence starts shortly before the onset of the jet and ends late in the decay phase. These images are from an XRT movie that views much of the northern polar coronal hole for several hours on 2008 September 20. In Figure 6, the jet is viewed in a small sub field of view of the movie. The movie was taken with the Thin Al Poly filter and has 1 minute cadence.

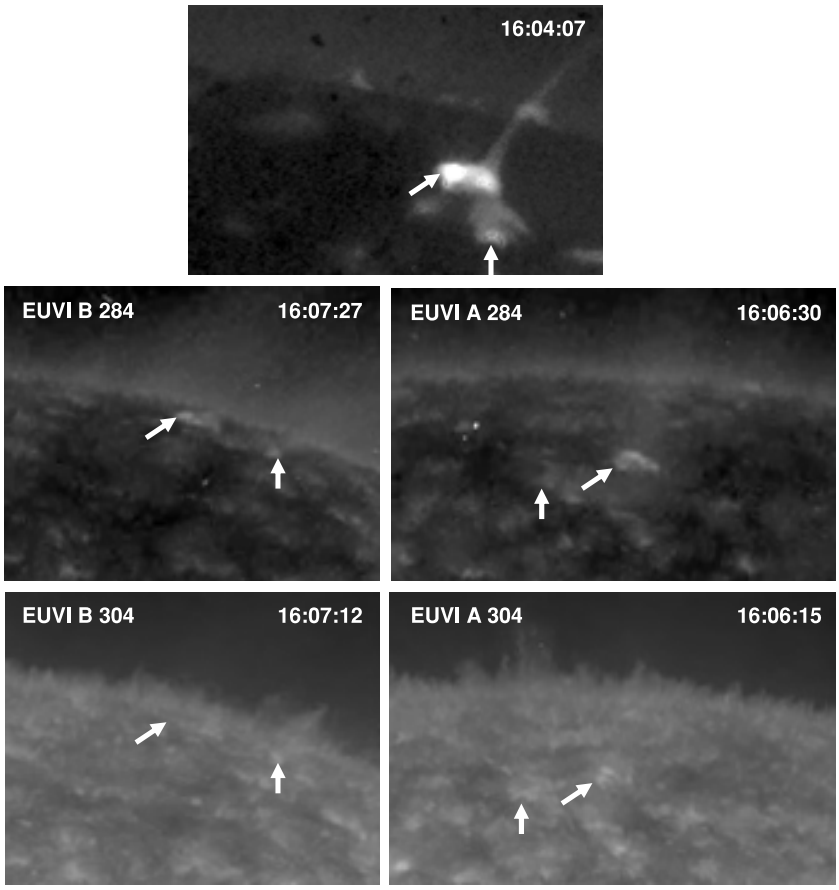

Figure 5. Co-temporal snapshots of the standard jet of 2008 October 5 showing that nearly all of the plasma in the jet's spire was hotter than $\sim 2 \times 10^6$ K. Top: XRT image of the jet and its surroundings in the northern polar coronal hole. This is a larger sub field of view taken from the same frame of the XRT movie as the seventh frame of Figure 4. It shows the jet when the spire and the bright point were at or near their maximum size and brightness. Middle left: EUVI B 284 Å image centered on the jet and covering a somewhat larger heliographic area than in the top image. Middle right: EUVI A 284 Å image centered on the jet and covering a somewhat larger heliographic area than in the top image. Bottom left: EUVI B 304 Å image of the same area viewed in the EUVI B 284 Å image above it. Bottom right: EUVI A 304 Å image of nearly the same area viewed in the EUVI A 284 Å image above it. In each image, the slanted arrow points to the location of the jet's bright point, the vertical arrow points to the location of the brightest small feature that is south of the jet's base in the XRT image, and the universal time is in the upper right corner. The angle of separation from Earth was 40° for *STEREO A* and 37° for *STEREO B*.

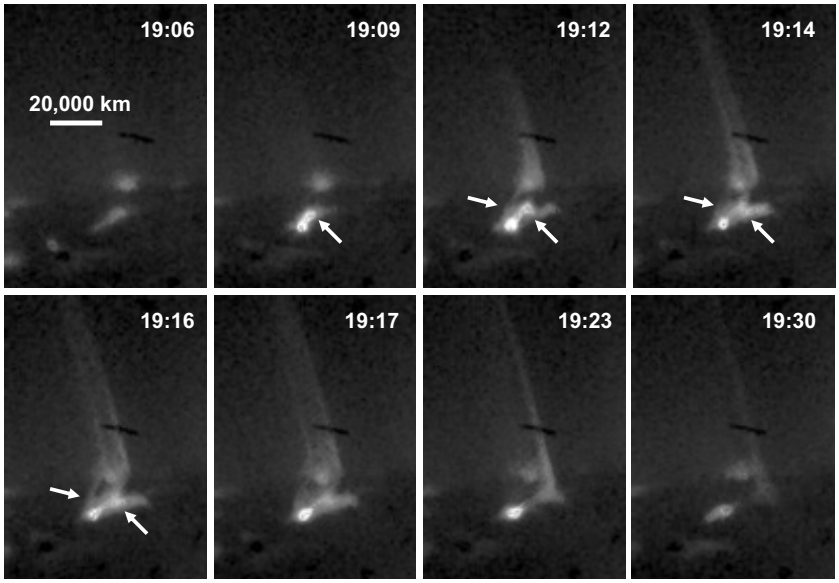

Figure 6. Progression of the blowout jet of 2008 September 20 observed in coronal X-ray images from *Hinode*/XRT. The jet's base arch is just inside the limb in the northern polar coronal hole, is viewed mostly from the side, and during the jet (third and later frames) is seen to span about 20,000 km. Each upward slanted arrow points to brightening in the interior of the base arch. Each downward slanted arrow points to the lower leg of a strand of the jet's spire that seems to be rooted in front of the jet's miniature-flare-arcade bright point. In the upper right corner of each frame is the universal time.

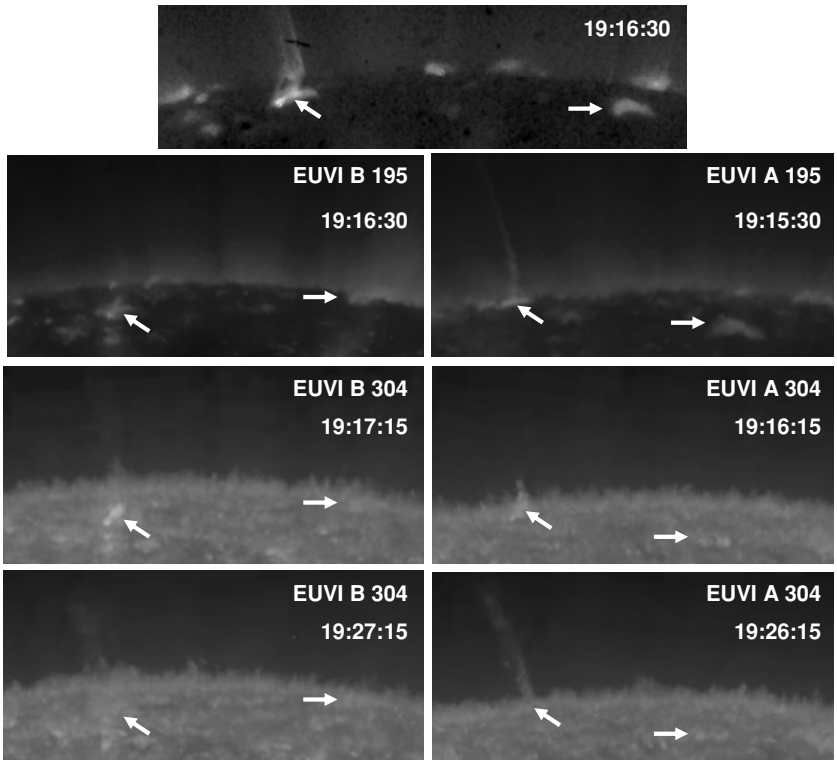

Figure 7. Snapshots of the blowout jet of 2008 September 20 showing that during the production of the X-ray jet much cooler ($T \sim 80{,}000$ K) plasma erupted from the jet's base and ejected along the spire of the X-ray jet. The upper five snapshots are nearly co-temporal in the jet's maximum phase; the bottom two are 10 minutes later, in the decay phase. Top: XRT image of the jet and its surroundings in the northern polar coronal hole. This is a larger sub field of view taken from the same frame of the XRT movie as the fifth frame of Figure 6. It shows the jet when the jet's two non-standard features, the front strand of the spire and the transiently bright interior of the base arch, are near their maximum brightness and size. Upper middle left: EUVI B 195 Å image of about the same heliographic area viewed in the top image. Upper middle right: EUVI A 195 Å image of about the same heliographic area. Lower middle left: EUVI B 304 Å image of nearly the same area viewed in the EUVI B 195 Å image above it. Lower middle right: EUVI A 304 Å image of nearly the same area viewed in the EUVI A 195 Å image above it. Bottom left: EUVI B 304 Å image of the same area viewed in the EUVI B 304 Å image above it. Bottom right: EUVI A 304 Å image of the same area viewed in the EUVI A 304 Å image above it. In each frame, the slanted arrow points to the base of the jet, the horizontal arrow points to the location of the dim arch seen inside the limb near the west edge of the top image, and the universal time is shown on the right, above the limb. The angle of separation from Earth was 39° for *STEREO A* and 35° for *STEREO B*.

In the first frame of Figure 6, the jet has not yet started, and much of the base arch is not bright enough to be seen. The base arch spans about 20,000 km, but that is not seen until the jet is in its maximum phase (e.g., fifth frame). Comparison of the first frame with the frame below it, the fifth frame, shows that the brightest feature in the jet's base in the first frame is a low arch less than 10,000 km long in the core of the jet's base. In the second frame, 3 minutes later, the jet's miniature-flare-arcade bright point has appeared at the southeast end of the base arch, and most of the low interior arch has become nearly as bright as the bright point, but the jet's spire is still too faint to be seen. In the third frame, another 3 minutes later, the brightening in the interior of the base arch has spread toward the northwest end of the base arch, and the jet's spire has become apparent. The jet now shows two striking features that are at odds with the standard model: (1) the brightening low in the interior of the base arch, and (2) instead of being rooted entirely toward the end of the base arch away from the bright point as in our two example standard jets, this jet's spire has an extra strand that is rooted near the bright-point end of the base arch. The foot of this strand appears to be in front of the bright point, putting the strand's field lines upstream from the reconnection patch in the standard model, so that this strand of the spire should have not yet undergone heating by the reconnection. In this way, the front strand of the spire appears to directly contradict the standard model. That the interior of the base arch brightened in X-ray emission in synchrony with the production of the jet suggests that in this jet the interior of the base arch actively participated in the eruption rather than remaining inert as in the standard model.

During the next 4 minutes after the third frame of Figure 6 (fourth and fifth frames), the spire becomes more curtain-like than the single-strand spires of our two example standard jets, the spire's non-standard front strand becomes brighter and more distinct, and the brightening in the interior of the base arch becomes more extensive. A minute later (sixth frame), the non-standard strand and the bright interior of the base arch have started to fade. Later in the decay phase (seventh and eighth frames), the front strand and curtain of the spire have faded away and the jet shows only the structure of a standard jet: a single-strand spire rooted at the end of the base arch opposite to the bright point. As can be seen from the changing position of the center line of the spire relative to the small bright feature on the limb behind the spire, the fading out of the spire's front strand and curtain gives the spire an apparent lateral migration away from the bright point.

Figure 7 shows that this jet also differed from our two example standard jets in that, in addition to the X-ray-emitting hot plasma in the jet's spire, plasma that was much cooler ($T \sim 80{,}000$ K) was ejected up along the same path from the base of the jet. The upper five snapshots in Figure 7 are all in a 1.75 minute interval in the maximum phase of the X-ray jet. The EUVI B Fe XII 195 Å image shows the bright base of the jet, and faintly shows only the lower leg of the spire inside the limb. The EUVI A

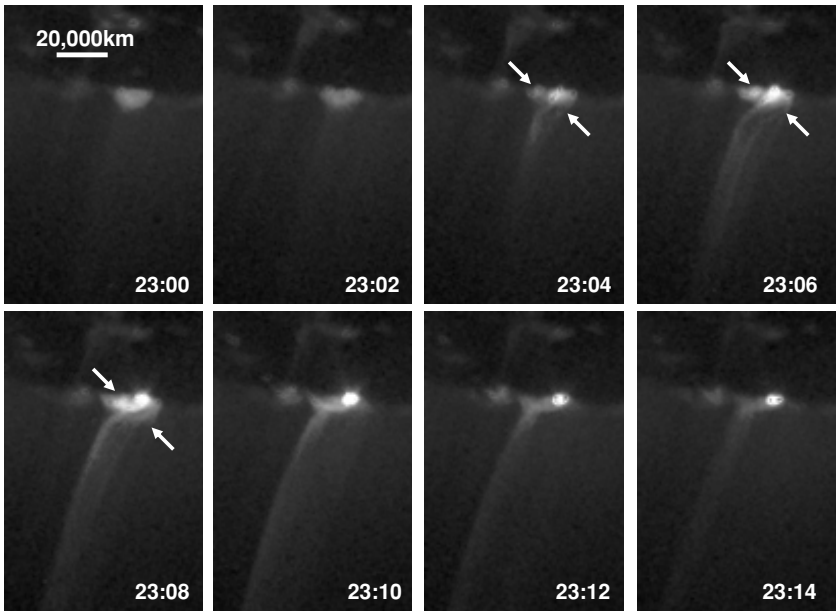

Figure 8. Progression of the blowout jet of 2008 December 4 observed in coronal X-ray images from *Hinode*/XRT. The jet's base arch is at the limb in the southern polar coronal hole, appears to be viewed mostly from the side, and spans about 15,000 km in the plane of the sky. Each southward slanted arrow points to brightening in the interior of the base arch. Each northward slanted arrow points to the lower leg of the front strand or front edge of the jet's spire, which edge appears to be rooted west of the jet's miniature-flare-arcade bright point at the west end of the base arch. The universal time is in the lower right corner of each frame.

Fe XII 195 Å image, probably because EUVI A viewed the spire more nearly edge-on than did EUVI B, in addition to showing the bright base of the jet, definitely shows the spire extending high into the corona above the limb. So, at this time there was appreciable plasma in the spire at a temperature of $\sim 1.5 \times 10^6$ K. This could be previous X-ray plasma that cooled to this temperature. The EUVI A He II 304 Å image at 19:16:15 UT, 45 s after the EUVI A Fe XII 195 Å image above it, shows both the jet's bright base (which sits on the limb from the perspective of EUVI A, as can be seen in the EUVI A 195 Å image) and bright He II plasma extending low into the X-ray spire to a height of ~20,000 km above the base. A minute later, in the EUVI B He II 304 Å image at 19:17:15 UT, this bright extension of He II plasma (which is wider and fainter in this perspective) is seen to have roughly doubled in height. So, these two He II snapshots show that transition-region-temperature plasma erupted from the base of the X-ray jet and moved up along the X-ray spire at a speed of ~300 km s^{-1}. Ten minutes later, the base of the jet has become too faint to be clearly seen in either of the bottom two EUVI He II snapshots in Figure 7, but in the EUVI A image He II plasma is definitely seen along the path of the X-ray spire to a height of ~100,000 km, consistent with the ~300 km s^{-1} speed of the He II jet estimated from the first two He II snapshots. In the bottom EUVI B 304 Å image, taken only a minute after the bottom EUVI A 304 Å image, the He II jet is wider and fainter than in the bottom EUVI A 304 Å image. Again, this is probably due to the different perspectives of EUVI A and EUVI B. Some of the He II plasma seen along the spire in the bottom two images in Figure 7 could be the cooled remnant of previous X-ray plasma in the spire. Even so, the four He II snapshots together strongly suggest that much of the He II plasma seen along the spire in the bottom two images is ejected transition-region-temperature plasma that erupted from the base of the jet. Figures 6 and 7 together show that the He II plasma eruption was delayed relative to the X-ray jet. The X-ray jet was already fully developed and reached far above the limb when the erupting He II plasma seen in the first EUVI A 304 Å image had reached only a little above the limb. The time lag suggests that the He II plasma eruption was triggered by the X-ray jet and/or started more slowly and from lower in the base than did the X-ray jet.

Because the base arch of the X-ray jet spanned ~20,000 km, the reconnection that produced the miniature-flare-arcade bright point probably occurred in the low corona rather than in or below the transition region. So it is unlikely that the He II plasma was ejected by the reconnection for standard jets. From this consideration, together with the delay of the He II plasma eruption relative to the X-ray jet and the common occurrence of erupting-loop Hα macrospicules, we surmise that in this jet the He II plasma erupted from low in the base arch as in an ejective filament eruption.

3.2. Blowout X-ray Jet of 2008 December 4

The sequence of coronal X-ray images in Figure 8 shows the development of our second example blowout jet. The sequence starts about 2 minutes before the onset of the jet and ends midway in the decay phase. These images are from an XRT movie that views most of the southern polar coronal holes for several hours on 2008 December 4. In Figure 8, the jet is viewed in a small sub field of view of the movie. The movie was taken with the Ti Poly filter at a cadence of 2 minutes. The plasma temperature response of the Ti Poly filter is similar to that of the Thin Al Poly filter in being most sensitive to plasma in the $5–10 \times 10^6$ K temperature range and very insensitive to plasma cooler than $\sim 10^6$ K (Kano et al. 2004).

In the first frame of Figure 8, the jet has not yet started, and the eastern leg of the base arch is a little brighter than the western leg. Two minutes later (second frame), the eastern leg has dimmed a little, the west end of the base arch is slightly brighter than its east end, and the jet's spire is becoming marginally visible, stemming from the eastern leg of the base arch. Two minutes later (third frame), the jet's miniature-flare-arcade bright point, which is barely starting to be visible in the previous frame, stands out near the west end of the base arch. The spire is now much

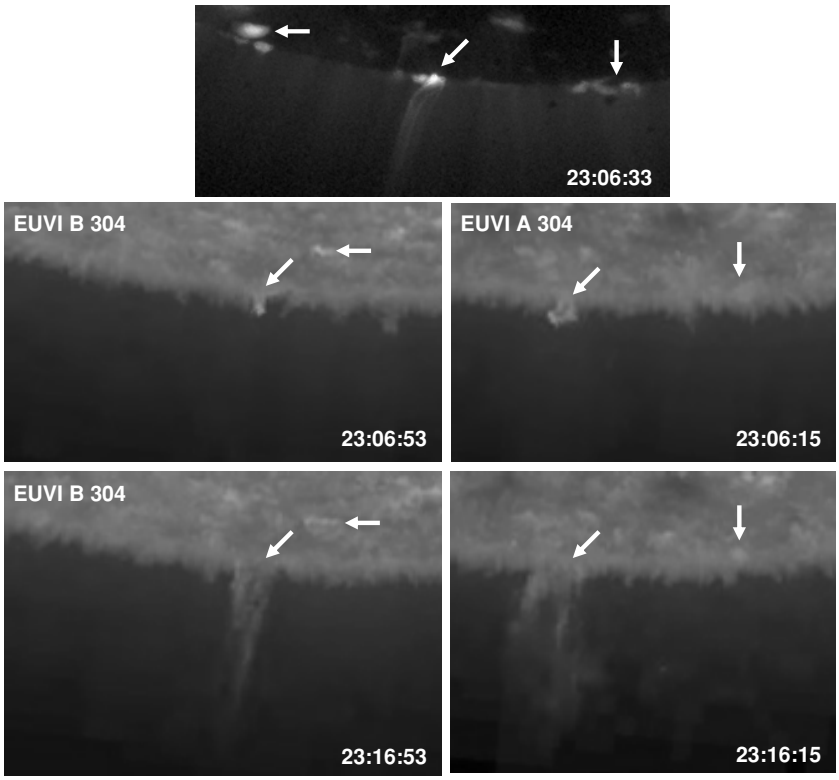

Figure 9. Snapshots of the blowout jet of 2008 December 4 showing that during the production of the X-ray jet an ejective filament eruption from the base of the jet, carrying transition-region-temperature ($T \sim 80{,}000$ K) plasma, exploded out along the spire of the X-ray jet. The upper three snapshots are nearly co-temporal. These catch the jet as it was entering its maximum phase. The bottom two snapshots are 10 minutes later, late in the decay of the X-ray jet. Top: XRT image of the jet and its surroundings in the southern polar coronal hole. This is a larger sub field of view taken from the same frame of the XRT movie as the fourth frame of Figure 8. It shows the jet when the jet's two non-standard aspects, strong brightening inside the base arch and a spire comprised of a curtain of strands with the front strand apparently rooted in front of the bright point, are both clearly seen and are rapidly getting brighter. Middle left: EUVI B 304 Å image of much of the heliographic area viewed in the top image. Middle right: EUVI A 304 Å image of much of the heliographic area viewed in the top image. Bottom left: EUVI B 304 Å image of the same area viewed in the EUVI B 304 Å image above it. Bottom right: EUVI A 304 Å image of the same area viewed in the EUVI A 304 Å image above it. The slanted arrows point to the base of the jet. The horizontal arrows point to the base of the bright arch seen near the east edge of the top image. The vertical arrows point to the base of a small bright feature seen at the limb near the west edge of the top image. The universal time is in the lower right corner of each frame. The separation angle from Earth was 42° for *STEREO A* and 44° for *STEREO B*.

more visible. Its main strand is rooted toward the eastern end of the base arch, away from the bright point as in a standard jet. But the spire also has a fainter curtain on its front side, toward the bright point. The front edge or front strand of the curtain appears to be rooted in front (west) of the bright point. Also in the third frame, the interior of the arch is seen to be brightening in the eastern leg of the base arch. During the next 4 minutes (fourth and fifth frames), the interior brightening increases and spreads throughout the base arch, the bright point grows bigger and brighter, both the main strand and the front curtain of the spire become brighter and more distinct, and the front strands of the curtain continue to be rooted in front of the bright point. During the next 6 minutes (sixth, seventh, and eighth frames), the spire's curtain and the base arch's bright interior fade out and the jet comes to have the form of a standard jet: a single-strand spire rooted at the end of the base arch away from the bright point.

This jet displays in its X-ray images in Figure 8 the same two non-standard features during its growth and maximum phase as our other example blowout jet displays in its X-ray images in Figure 6. Again, the spire's front edge appears to contradict the standard model by being rooted in front of the bright point, and the strong brightening in the interior of the base arch in step with the production of the jet suggests that the interior of the base arch was not basically inert as in the standard model but actively participated in the eruption.

Figure 9 establishes that in this jet the interior of the base arch indeed was not passive but became part of the jet by undergoing a "blowout," that is, by erupting in the manner of the eruptions that become major CMEs. The upper three snapshots in Figure 9 (one from XRT, one from EUVI A, and one from EUVI B), are all in a 0.63 minute interval early in the maximum phase of the X-ray jet. Both of these EUVI He II 304 Å snapshots show an erupting-loop filament erupting out of the base of the jet seen in the XRT snapshot. In these snapshots, the top of the loop has reached a height of no more than a few times the height of the pre-jet base arch seen in Figure 8. The image from EUVI A views the erupting loop enough side-on to the plane of the loop to show this protrusion to be a loop. The image from EUVI B apparently views the loop very nearly end-on, so that one leg of the loop is behind the other along the line of sight. Because the erupting loop seen in these He II 304 Å images appears similar to typical erupting-loop Hα macrospicules seen in Hα images, it presumably erupted from low in the jet's base arch, carried by erupting sheared core field as in a filament eruption in a CME eruption, as discussed in Yamauchi et al. (2004).

The bottom two snapshots in Figure 9 are He II 304 Å snapshots taken 10 minutes later by EUVI A and EUVI B. These show that the filament field and plasma erupted on up into the corona along the X-ray jet's spire at a speed of $\sim$100 km s^{-1} or more. In the first EUVI A image in Figure 9, at 23:06:15, the filament had risen to no more than about 20,000 km above the

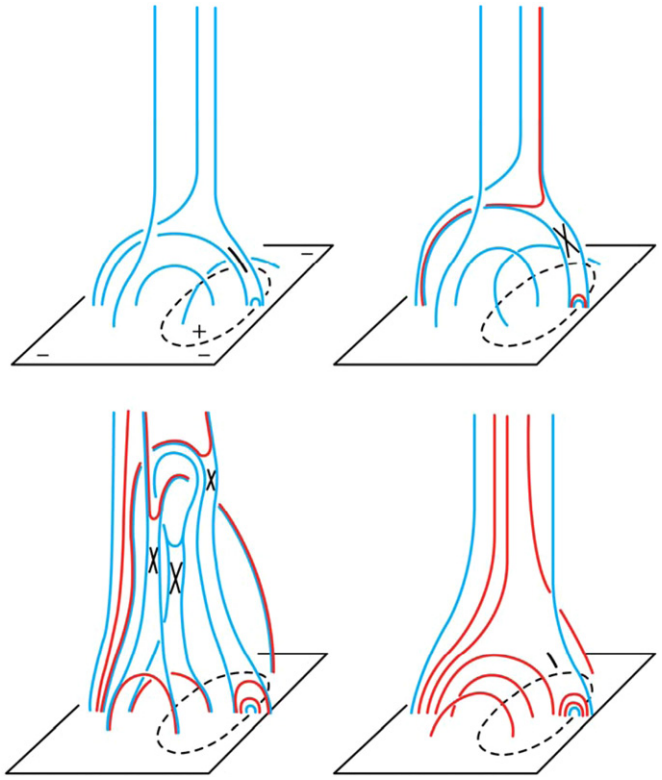

Figure 10. Schematic depiction of the topology, eruption, and reconnection of the magnetic field in our proposed model for blowout jets. Here, as in Figure 1 for standard jets, only a few representative field lines are drawn. Red field lines are those that have been reconnected; these have reconnection-heated X-ray plasma on them. Blue field lines either have not yet been reconnected or will not be reconnected. Top left: the field configuration before the eruption starts. As in Figure 1, the dashed oval is the polarity inversion line around the positive flux of the emerging magnetic arch, and the nearly unstable patch of the current sheet between the base arch and the ambient open field is represented by the curved black line. The field line arching low along the polarity inversion line in the middle of the base arch indicates that the field in the core of the arch is extremely sheared. The open field line in the foreground represents the open field that reconnects with the core field during the blowout eruption of the core field. Top right: onset of the breakout reconnection (marked by the X) as the sheared core field begins to erupt. Bottom left: reconnection and its heated field lines during the blowout eruption of the sheared-core base arch. Bottom right: the X-ray jet at the onset of its decay phase.

limb. So, its average upward speed in the 222 s interval from the very onset of the X-ray jet seen in the second frame of Figure 8 (at 23:02:33) to 23:06:15 in the X-ray jet's rapid growth phase was no more than $\sim$100 km s^{-1}. This is about right for the sheared core field carrying the filament to have begun erupting as the X-ray brightening inside the base arch turned on, and for the eruption to have accelerated rapidly as this brightening increased. Such coordination of flare brightening in the core of an erupting sheared-core magnetic arcade with the blowout eruption of the arcade is observed in the onsets of CME eruptions (Moore et al. 2001; Moore & Sterling 2006).

3.3. Schematic Model for Blowout Jets

The sequence of cartoons in Figure 10 depicts our concept for the production of blowout coronal jets. This scenario builds on the standard model depicted in Figure 1. In both cases, the magnetic field setup is the same in that there is a high-reaching ambient unipolar field into which a compact, low-arching, bipolar field is emerging from below the photosphere. The essential difference is that, whereas for a standard jet the emerging-arch field has no appreciable shear or twist in it, for a blowout jet the field in the core of the arch is so strongly sheared and twisted that it has enough free energy to drive an ejective eruption, a blowout of the arch, as in the blowout of the sheared-core magnetic arcade in a CME eruption.

The first drawing in Figure 10 corresponds to the first drawing in Figure 1. As in Figure 1, we have given the ambient open field negative polarity, so that again the intrusion of the emerging magnetic arch forces a current sheet to form at the interface between the ambient field and the positive-polarity leg of the arch. Also as in Figure 1, the short black curve at this interface in the pre-jet drawing in Figure 10 represents the patch of the current sheet that has become thin enough and extensive enough that it is on the verge of becoming unstable to reconnection. But this pre-jet drawing differs from the one in Figure 1 for standard jets in two ways. First, the core of the arch, the field that is rooted near the polarity inversion line inside the arch and that is represented in this drawing by a single field line, is shown to be extremely sheared rather than nearly potential. Second, an additional open field line is shown in this drawing, the one that is rooted beside the arch's negative-polarity flux and that is in the foreground.

The second drawing in Figure 10 (top right) shows the onset of the X-ray jet. This shows that a blowout jet starts in apparently the same way as a standard jet, by the onset of a burst of reconnection at the interface current sheet. This starts producing a single-strand spire together with a miniature-flare-arcade bright point as in a standard jet. This drawing also schematically shows the sheared core field starting to erupt as in a filament eruption. We suppose that just as in the triggering of a CME eruption when there is an external current sheet at which breakout reconnection can occur (Moore & Sterling 2006), there are two alternative possibilities for the triggering of a blowout-jet eruption. One alternative is that the interface current sheet becomes unstable to reconnection and reconnection starts there on its own. This amounts to breakout reconnection that removes some of the arch's outer field that helped to keep the sheared core field tied down and unable to erupt. In turn, the core field then starts to erupt upward, which drives more breakout reconnection, which further unleashes the core field, and so on, a la Antiochos (1998), resulting in the blowout eruption of the arch. Because the breakout reconnection starts first in this alternative, the jet's spire and bright point can start a little before any noticeable X-ray brightening in the core of the base arch. This appears to be the case in our second example blowout jet (Figure 8). The other alternative is that the sheared core field starts erupting on its own before any breakout reconnection has started at the interface current sheet. In this alternative, the eruption of the core field could be triggered by MHD instability of the sheared-core-field flux rope, or by tether-cutting reconnection of the legs of the sheared core field, or by both of these mechanisms acting in concert (Moore & Sterling 2006). But as the core field starts erupting, it immediately starts increasing the pressure on the interface current sheet and soon starts driving breakout reconnection there. This breakout reconnection further unleashes the eruption, and blowout again occurs as when the breakout reconnection started first. Because the core field starts erupting first in this alternative, the interior of the base arch can start brightening in X-ray images before the onset of the jet's bright point and spire. This was observed in our first example blowout jet: early brightening is evident in the core of the base arch in the XRT movie frame taken at 19:07 UT, not shown in Figure 6.

The next drawing in Figure 10 (bottom left) shows the blowout eruption of the base arch in progress later in the growth phase of the jet. Now reconnection occurs at three places. First, the reconnection that started at the interface current sheet early in the eruption continues at this interface as the arch's top explodes upward, stretching the arch's legs and raising the reconnection site. This reconnection continues to build the jet's bright point. Second, as in CME eruptions, either from the very start of the eruption or soon after the eruption of the core field is underway, reconnection starts and grows between the opposite-polarity stretched legs of the erupting base arch. Such reconnection is the internal tether-cutting reconnection described in Moore et al. (2001) and in Moore & Sterling (2006). In the bottom left drawing in Figure 10, this reconnection is indicated by the lowest of the three Xs. It produces a flare arcade that straddles the polarity inversion line inside the base arch, as is sketched in the drawing. Third, there is reconnection between the positive-polarity leg of the erupting core-field flux rope (represented in this drawing by a single field line) and the negative-polarity ambient open field that it pushes against (the open field represented by the additional open field line in the first and second drawings). The downward product of this reconnection is a flare loop that has its positive-polarity foot inside the erupting base arch. This flare loop adds to the nearby end of the flare arcade that forms farther inside the base arch. The upward product of this reconnection is schematically shown in this drawing to be a non-standard extra strand of the jet's spire, a strand that is rooted near the bright-point end of the base arch, and that in projection appears to be rooted slightly in front of the bright point in the plane of the sky. In this way, the blowout eruption of the sheared core field and its base-arch envelope, via these three venues of reconnection, sustains the jet's bright point, produces the X-ray brightening inside the base arch, and produces an X-ray spire that displays multi-stranded curtain structure, the front strand of which can appear to be rooted in front of the bright point, as in our two example blowout jets.

In either alternative for triggering the eruption, the breakout reconnection starts in the low corona on the outer edge of the base arch as the sheared core field carrying chromospheric and transition-region plasma from low in the core of the arch just starts to erupt, as sketched in the top right drawing in Figure 10. This is consistent with the observations in Figures 7 and 9 for our two example blowout jets: the He II 304 Å filament plasma did not erupt much above the height of the pre-jet base arch until after the X-ray jet had started.

The fourth drawing in Figure 10 (bottom right) portrays the blowout jet after the top of the erupting core-field flux rope and its envelope of base-arch field have escaped much higher than in the third drawing. The three strains of reconnection have now petered out, and the jet is early in its decay phase. A now stable current sheet is shown to again be present at the interface between the ambient open field and the positive-polarity leg of the now reclosed base arch. In the case depicted here, because all reconnection heating has stopped, the X-ray jet's spire and bright point and the X-ray bright interior of the base arcade will now cool and fade away in coronal X-ray images. In each of our two example blowout jets, the bright point and the spire's strand on the end of the base arch away from the bright point persist longer in the decay phase than do the bright interior of the base arch and the spire's front strand and curtain. This is compatible with our scenario if, instead of having the reconnection at the interface stop in step with the other two strains of reconnection at the start of the decay phase, as we do in the bottom right drawing in Figure 10, we have it persist for some time into the decay phase, reconnecting ambient open field with the positive leg of the reclosed base arch after the other two strains have stopped.

4. SUMMARY AND DISCUSSION

From the structure and development of X-ray jets observed in *Hinode*/XRT coronal X-ray movies of the Sun's polar coronal holes, we found that nearly all solar polar X-ray jets appear to be one or the other of two different types. About two thirds are standard jets and about a third are blowout jets. The standard X-ray jets are evidently produced by reconnection between an emerging magnetic arch at the base of the jet and the ambient unipolar open magnetic field of the coronal hole, during which the interior of the base arch is inert and does not participate in the eruption. The blowout X-ray jets correspond to erupting-loop Hα macrospicules and are evidently produced by blowout eruption of the base arch, a miniature version of the blowout eruption of the sheared-core magnetic arcade in a CME eruption. In this paper, for two typical standard X-ray jets and two typical blowout X-ray jets, we have presented evidence from *Hinode*/XRT coronal X-ray images in combination with *STEREO*/EUVI coronal and transition-region EUV images that each of these jets was produced in the way expected for its type.

From the presented observations of our four example jets, interpreted with the standard reconnection model for standard jets and our proposed model for blowout jets, we expect that (1) most standard X-ray jets having base arches spanning $\sim$20,000 km or more should be hardly or not at all visible in images of emission from plasma at temperatures less than $\sim 10^6$ K, and (2) most blowout X-ray jets should also be evident in EUV and Hα emission from transition-region and chromospheric plasma carried in the blowout eruption of the sheared core field of the base arch. The present study does not establish whether either of these expectations is actually true. The fraction of standard X-ray jets that are also evident in images of emission from plasma at subcoronal temperatures and the fraction of blowout X-ray jets that are not evident in such images remain to be determined from a much larger sample of X-ray jets that have suitable coverage in EUV and/or Hα movies. On the positive side, we think that the observations presented in this paper do make a strong case that there is a dichotomy of coronal jets (standard jets and blowout jets) due to a dichotomy of the production process, which is whether the core of the magnetic arch at the jet's base remains inert as the jet is produced or undergoes a blowout eruption that drives the production of the jet.

High-resolution magnetograms from NSO/Kitt Peak, from *SOHO*/MDI, and from *Hinode*/SOT have shown that the number of small emerging magnetic bipoles in quiet regions and coronal holes increases rapidly with decreasing size, at least down to those having arch spans as short as 2–3 $\times$ 10^3 km (Falconer et al. 1998; Hagenaar 2001; Parnell et al. 2009). That is, there are vastly more emerging magnetic arches that are too small to arch into the low corona, or to even arch above the chromospheric base of the spicule forest, than there are emerging magnetic arches that are large enough to arch into the low corona, which the base arches of most X-ray jets do. The observed dichotomy of both X-ray jets and Hα macrospicules and that the base width of many Hα macrospicules of either type is as small as 10,000 km imply that at least down to this size there is a dichotomy of emerging magnetic arches: those that do not have enough magnetic shear and twist to have a blowout eruption and those that do.

This dichotomy plausibly extends to smaller emerging magnetic arches, including those small enough to make chromospheric jets of the size of spicules. By this reasoning, from the dichotomy of coronal jets we infer that there is a large class of spicules that are chromospheric standard jets and another large class of spicules that are chromospheric blowout jets.

If the blowout eruption of the base arch in blowout X-ray jets and in erupting-loop macrospicules is a miniature version of the blowout eruptions that produce CMEs, then the erupting plasmoid in these blowout coronal jets should expand laterally as it escapes upward in the ambient field (Moore et al. 2007). This evidently happened in our two example blowout X-ray jets: the images in Figures 7 and 9 show that in each of these blowout eruptions the base-arch field carrying the He II filament plasma definitely expanded laterally as it erupted up along spire of the X-ray jet. From a *Hinode*/SOT Ca II movie of the chromosphere at the limb in a coronal hole, Sterling et al. (2010) recently found that some fast spicules expand laterally as they erupt into the high chromosphere, in a manner reminiscent of filament eruptions. This observation bolsters the inference from our results that (1) there is a large class of spicules that are chromospheric blowout jets made by the blowout eruption of magnetic arches of (2–3) $\times$ 10^3 km long or smaller, and (2) there is a comparably large class of spicules that are chromospheric standard jets, having non-eruptive base arches that are as small as the eruptive base arches for blowout spicules.

The present paper is not the first to present coronal jets for which there is good evidence for blowout eruption of the base arch as in our two example blowout jets, and is not the first to propose that for such coronal jets the interior of the pre-jet closed field at the base is strongly sheared and twisted, and that blowout eruption of this contorted field is unleashed by breakout reconnection of the outside of the closed field with the ambient open field. Wang et al. (1998) found 27 coronal jets that occurred in the polar coronal holes, were observed in sequences of full-disk Fe XII 195 Å coronal images from *SOHO*/EIT, and were observed later beyond 1 $R_{\rm Sun}$ above the limb in sequences of white-light images from the *SOHO*/LASCO/C2 coronagraph. The elapsed time between eruption from the base and arrival in the C2 field of view gave speeds in the range 3–7 $\times$ 10^2 km s^{-1} for these jets. These speeds are similar to those of polar X-ray jets observed by *Yohkoh*/SXT and *Hinode*/XRT (Shimojo et al. 1996; Savcheva et al. 2007; Cirtain et al. 2007). Nine of these 27 jets are shown in EIT 195 Å images in Wang et al. (1998). In these images, only one of these jets appears to have the structure of a standard jet. The rest show structure like that of blowout X-ray jets, and two of these appear to be erupting in the manner of the He II filament eruptions in our two example blowout jets. So we think that of these nine jets, two definitely were blowout jets and six others probably were.

Patsourakos et al. (2008) present a coronal jet that occurred nearly at the limb in the northern polar coronal hole and that was well observed by both EUVI A and EUVI B in sequences of 171 Å, 195 Å, and 304 Å images. The 171 Å images see Fe IX/X line emission from plasma at temperatures of $\sim$1 $\times$ 10^6 K (Howard et al. 2008), and during this jet they have a 2.5 minute cadence. The 171 Å images show the blowout eruption of a filament-like loop structure from inside the base of the jet. This loop starts rising slowly from low in the base as the jet's bright point turns on at the outer edge of the base. Then the loop top accelerates rapidly and the loop erupts "open," as in the blowout eruption of an erupting-loop Hα macrospicule. The He II 304 Å images have a 10 minute cadence. One of these snapshots catches the jet as the erupting filament seen in the 171 Å movie is blowing open. It shows that much of the plasma carried in the erupting field was cool (T $\sim$ 80,000 K), in agreement with the field having erupted from low in the base. The Patsourakos et al. (2008) paper points out that this eruption behaved much like an MHD simulation of such an eruption that was developed and studied by two of the co-authors (E. Pariat and S. K. Antiochos) and that was subsequently presented in detail by Pariat et al. (2009). In this simulation, the closed base field is axisymmetric so that the interior field can be sheared to a very large degree before an MHD instability sets in that breaks the symmetry and allows breakout reconnection to begin. This model is too artificial to realistically simulate either the onset of the breakout reconnection or the size and growth of the observed jet's bright point, but it does nicely demonstrate the sheared internal field's blowout unleashed by the breakout reconnection. In a follow-up paper, by using a pair of numerical simulations, in one of which reconnection is allowed and in the other of which reconnection is entirely prevented, Rachmeler et al. (2010) show that in this axisymmetric model for blowout jets breakout reconnection is necessary for the MHD instability of the sheared core field to result in the production of a jet.

The observations presented in Wang et al. (1998), Yamauchi et al. (2004), and Patsourakos et al. (2008) show that blowout jets occur. The observations presented in Patsourakos et al. (2008) together with the MHD simulation of Pariat et al. (2009) make a strong case that blowout jets are driven by blowout eruption of strongly sheared field from the base via breakout reconnection with the ambient open field. Our intent in the present paper was not mainly to show that blowout jets happen and that they are unleashed by breakout reconnection. The purpose of this paper is to (1) emphasize that while many polar coronal jets are blowout jets, at least as many are standard jets, and nearly all are one or the other; (2) from their observed signatures in coronal X-ray images, identify which X-ray jets are standard jets and which are blowout jets; (3) infer how these signatures result from the production process; and (4) point out the implication of the observed dichotomy of coronal jets for the production of spicules.

In the present study, the primary observations of coronal jets were from *Hinode*/XRT movies of the polar coronal holes. These X-ray movies of $\sim$100 jets were supplemented with EUV snapshots from *STEREO*/EUVI for four X-ray jets selected for their fortuitous capture in EUVI He II 304 Å snapshots. There are three other recent observational studies of coronal jets that have found similar or complementary evidence that some coronal jets are miniature CME eruptions. Two of these studies are based primarily on EUV movies from EUVI of the transition region and corona, and one is based primarily on *Hinode*/XRT movies. Nistico et al. (2009) studied 79 coronal jets that occurred in the polar coronal holes and were observed by the EUVI imager and by the COR1 coronagraph of the SECCHI instrument package (Howard et al. 2008) on both *STEREO A* and *STEREO B*. They found that the majority of these (49) were standard jets, and that of the remaining 30, although most (25) were ambiguous, 5 clearly showed "filament eruptions" indicating that the jet was basically a micro-CME eruption. In a very recent study of two coronal jets, each of which was observed on the limb in a He II 304 Å movie from EUVI B and simultaneously on the central disk in a Fe IX/X 171 Å movie from EUVI A, Innes et al. (2010) found that in each jet coronal dimming preceded the onset of the ejection of the He II plasma, consistent with a mini-CME eruption initiated by breakout reconnection of the

erupting field with surrounding high-reaching coronal field. In the third recent study, this one based mainly on *Hinode*/XRT movies of the polar coronal holes, Raouafi et al. (2010) found clear evidence of micro-sigmoid core fields that undergo micro-CME eruptions (blowout jets). The observed sigmoid structures verify the presence of a strongly sheared/twisted core field in the pre-eruption jet-base arch in blowout jets, more or less as we depict in Figure 10.

In estimating the relative population of standard jets and blowout jets, we judged a jet to be a standard jet or a blowout jet or ambiguous entirely from the XRT images, without examining EUVI images of the jet. Of the 55 X-ray jets that we examined for this estimate, none of the 34 identified standard jets had curtain-like spires and none had increasing brightness inside the base arch as the jet spire turned on and grew. Each of the 18 identified blowout jets had both of these features. Therefore, we are confident that few if any of the jets that appeared to be standard jets were actually blowout jets. From the above examination of 79 EUV coronal jets by Nistico et al. (2009), from the examination of 35 Hα macrospicules by Yamauchi et al. (2004), and from our examination of 55 X-ray jets, we conclude that in polar coronal holes (1) at least half of all coronal jets are standard jets, (2) about two thirds of coronal X-ray jets are standard jets, and (3) about one third of coronal X-ray jets are blowout jets.

Finally, we point out that the dichotomy of coronal jets might be evident in the white-light polar coronal jets observed in the outer corona, such as those reported by Wang et al. (1998). In major CMEs, the erupting magnetic arcade with a twisted flux rope in its core soon enters open field in the upper corona. It then becomes likely that interchange occurs, reconnection of the open field with the outer edge of the CME where the direction of the CME's field is opposite to that of the ambient open field (Crooker & Siscoe 2004). But there is ample magnetic flux in a major CME for the plasmoid and its interior flux rope to survive to well beyond 1 AU, remaining mostly unopened by the interchange reconnection. The interchange reconnection is topologically the same as the breakout reconnection in blowout jets. In polar blowout jets, the amount of flux in the erupting field is orders of magnitude less than in major CMEs. So, it seems likely that the outer envelope of the erupting base arch, which has little shear or twist, is soon opened by the breakout/interchange reconnection, and this reconnection then eats into the strongly twisted erupting flux rope inside. This would transfer the flux rope's twist onto the reconnected open field lines, twist which would then propagate out along the open field like a torsional Alfvèn wave. Such upward escaping twist on open field lines is apparently observed in the blowout jet of Patsourakos et al. (2008), and occurs in the MHD simulation of Pariat et al. (2009). Rust et al. (2009) have found from wavelet processing of LASCO/C2 images that coronal "steamers" rooted in coronal holes near flaring active regions sometimes show outward-propagating twist. From these results and the dichotomy of coronal jets, we expect that there is a corresponding dichotomy of the white-light jets in the outer corona: those that have hardly any twist and come from standard jets at their feet, and those that have appreciable twist and come from blowout jets.

This work was funded by NASA's Science Mission Directorate through the Heliophysics Guest Investigators Program, the *Hinode* Project, and the Living With a Star Targeted Research & Technology Program. We thank the referee for helpful comments that resulted in making the paper clearer and in making the paper more cognizant of recent related published or submitted papers on coronal jets.

REFERENCES

Antiochos, S. K. 1998, ApJ, 502, L181
Axford, W. I., & McKenzie, J. F. 1992, in Solar Wind Seven, ed. E. Marsch & R. Schwenn (Oxford: Pergamon), 1
Beckers, J. M. 1968, Sol. Phys., 3, 367
Beckers, J. M. 1972, ARA&A, 10, 73
Cirtain, J. W., et al. 2007, Science, 318, 1580
Crooker, N. C., & Siscoe, G. L. 2004, AGU 2004 Fall Meeting, abstract SM43B-05 (Washington, DC: AGU)
DeLuca, E. E. 2007, in ASP Conf. Ser. 369, New Solar Physics with Solar-B Mission, ed. K. Shibata, S. Nagata, & T. Sakurai (San Francisco, CA: ASP), 19
De Pontieu, B., et al. 2007, PASJ, 59, S655
Falconer, D. A., Moore, R. L., Porter, J. G., & Hathaway, D. H. 1998, ApJ, 501, 386
Falconer, D. A., Moore, R. L., Porter, J. G., & Hathaway, D. H. 2003, ApJ, 593, 549
Fisk, L., Schwadron, N. A., & Zurbuchen, T. H. 1999, J. Geophys. Res., 104, 19765
Hagenaar, H. J. 2001, ApJ, 555, 448
Heggland, L., De Pontieu, B., & Hansteen, V. H. 2009, ApJ, 702, 1
Howard, R. A., et al. 2008, Space Sci. Rev., 136, 67
Innes, D. E., McIntosh, S. W., & Pietarila, A. 2010, A&A, submitted (arXiv: 1005.2097v1)
Kano, R., et al. 2004, in ASP Conf. Ser. 325, The Solar-B Mission and the Forefront of Solar Physics, ed. T. Sakurai & T. Sekii (San Francisco, CA: ASP), 15
McIntosh, S. W., Davey, A. R., Hassler, D. M., Armstrong, J. D., Curdt, W., Wilhelm, K., & Lin, G. 2007, ApJ, 654, 650
Moore, R. L., Falconer, D. A., Porter, J. G., & Suess, S. T. 1999, ApJ, 525, 505
Moore, R. L., Musielak, Z. E., Suess, S. T., & An, C.-H. 1991, ApJ, 378, 347
Moore, R. L., & Sterling, A. C. 2006, in Solar Eruptions and Energetic Particles, ed. N. Gopalswamy, R. Mewaldt, & J. Torsti (Washington, DC: AGU), 43
Moore, R. L., Sterling, A. C., Hudson, H. S., & Lemen, J. R. 2001, ApJ, 552, 833
Moore, R. L., Sterling, A. C., & Suess, S. T. 2007, ApJ, 668, 1221
Moreno-Insertis, F., Galsgaard, K., & Ugarte-Urra, I. 2008, ApJ, 673, L211
Nistico, G., Bothmer, G., Patsourakos, S., & Zimbardo, G. 2009, Sol. Phys., 259, 87
Pariat, E., Antiochos, S. K., & De Vore, C. R. 2009, ApJ, 691, 61
Parker, E. N. 1991, ApJ, 372, 719
Parnell, C. E., DeForest, C. E., Hagenaar, H. J., Johnston, B. A., Lamb, D. A., & Welsch, B. T. 2009, ApJ, 698, 75
Patsourakos, S., Pariat, E., Vourlidas, A., Antiochos, S. K., & Wuelser, J. P. 2008, ApJ, 680, L73
Porter, J. G., & Moore, R. L. 1988, in Solar and Stellar Coronal Structure and Dynamics, ed. R. C. Altrock (Sunspot, NM: National Solar Observatory, Sacramento Peak), 125
Rabin, D., & Moore, R. L. 1980, ApJ, 241, 394
Rachmeler, L. A., Pariat, E., DeForest, C. E., Antiochos, S., & Torok, T. 2010, ApJ, 715, 1556
Raouafi, N.-E., Georgoulis, M. K., Rust, D. M., & Bernasconi, P. N. 2010, ApJ, submitted (arXiv:1005.4042v1)
Roberts, D. A. 2010, ApJ, 711, 1044
Rouppe van der Voort, L., Leenaarts, J., De Pontieu, B., Carlsson, M., & Vissers, B. 2009, ApJ, 705, 272
Rust, D. M., Haggerty, D. K., Georgoulis, M. K., & Stenborg, G. 2009, BAAS, 41, 865
Savcheva, A., Cirtain, J. W., Deluca, E. E., & Golub, L. 2009, ApJ, 702, L32
Savcheva, A., et al. 2007, PASJ, 59, S771
Schrijver, C. J., et al. 1998, Nature, 394, 152
Shibata, K. 2001, in Encyclopedia of Astronomy and Astrophysics, ed. P. Murdin (Bristol: IOP Publishing), 3258
Shibata, K., et al. 1992, PASJ, 44, L173
Shimojo, M., Hashimoto, S., Shibata, K., Hirayama, T., Hudson, H. S., & Acton, L. W. 1996, PASJ, 48, 123
Sterling, A. C. 2000, Sol. Phys., 196, 79
Sterling, A. C., Moore, R. L., & DeForest, C. E. 2010, ApJ, 714, L1
Wang, Y.-M., et al. 1998, ApJ, 508, 899
Yamauchi, Y., Moore, R. L., Suess, S. T., Wang, H., & Sakurai, T. 2004, ApJ, 605, 511
Yokoyama, T., & Shibata, K. 1996, PASJ, 48, 353